The effect of eccentricity and spatiotemporal energy on motion silencing

Lark Kwon Choi
Department of Electrical and Computer Engineering, The University of Texas at Austin, Austin, TX, USA

Alan C. Bovik
Department of Electrical and Computer Engineering, The University of Texas at Austin, Austin, TX, USA

Lawrence K. Cormack
Department of Psychology, Institute for Neuroscience, and Center for Perceptual Systems, The University of Texas at Austin, Austin, TX, USA

The now well-known motion-silencing illusion has shown that salient changes among a group of objects' luminances, colors, shapes, or sizes may appear to cease when objects move rapidly (Suchow & Alvarez, 2011). It has been proposed that silencing derives from dot spacing that causes crowding, coherent changes in object color or size, and flicker frequencies combined with dot spacing (Choi, Bovik, & Cormack, 2014; Peirce, 2013; Turi & Burr, 2013). Motion silencing is a peripheral effect that does not occur near the point of fixation. To better understand the effect of eccentricity on motion silencing, we measured the amount of motion silencing as a function of eccentricity in human observers using traditional psychophysics. Fifteen observers reported whether dots in any of four concentric rings changed in luminance over a series of rotational velocities. The results in the human experiments showed that the threshold velocity for motion silencing almost linearly decreases as a function of log eccentricity. Further, we modeled the response of a population of simulated V1 neurons to our stimuli. We found strong matches between the threshold velocities on motion silencing observed in the human experiment and those seen in the energy model of Adelson and Bergen (1985). We suggest the plausible explanation that as eccentricity increases, the combined motion-flicker signal falls outside the narrow spatiotemporal frequency response regions of the modeled receptive fields, thereby reducing flicker visibility.

Introduction

The salient changes of objects in luminance, color, size, or shape may appear to reduce or to cease altogether when the objects move rapidly and collectively (Suchow & Alvarez, 2011). In the study by Suchow and Alvarez (2011), 100 small dots were randomly arranged in a ring-shaped pattern around a central fixation mark (the illusion may be viewed at http://visionlab.harvard.edu/silencing/.). When the dots are stationary, continuous changes over time in luminance, color, size, or shape are obviously noticeable; however, when the dots are suddenly sent into continuous rotational motion, the changes become imperceptible. This motion-induced failure to detect change, known as *motion silencing*, shows that motion can disrupt the perception of changes in visual objects.

Motion silencing clearly depends on the velocity of motion (Suchow & Alvarez, 2011), and it has since been shown that motion silencing also depends on dot spacing in a manner consistent with crowding (Turi & Burr, 2013) and on flicker frequency combined with motion and dot spacing (Choi, Bovik, & Cormack, 2014). Turi and Burr (2013) proposed that the combination of global motion and crowding results in motion silencing and presented evidence that silencing depends on target-flanker spacing with a critical spacing of about half eccentricity, consistent with Bouma's law (Bouma, 1970) and on contrast polarity. Choi et al. (2014) suggested that a spatiotemporal filter-based flicker detector model can explain motion silencing as a function of stimulus velocity, flicker frequency, and spacing between dots. Peirce (2013) examined whether the awareness of motion signals can be silenced by coherent changes in color or size and whether coherence was a necessary component of motion silencing. His results suggest that neither motion nor grouping is required to induce silencing and

Citation: Choi, L. K., Bovik, A. C., & Cormack, L. K. (2016). The effect of eccentricity and spatiotemporal energy on motion silencing. *Journal of Vision*, *16*(5):19, 1–13, doi:10.1167/16.5.19.

doi: 10.1167/16.5.19 Received September 28, 2015; published March 28, 2016. ISSN 1534-7362

that silencing can be generated from other significant visual changes (Peirce, 2013). Although these studies have substantially contributed to our understanding of what factors contribute to motion silencing, the effect of eccentricity on motion silencing has not yet been extensively studied. Because silencing is largely a peripheral effect, the role of eccentricity is highly relevant. Thus far, eccentricity has been used only in a subsidiary manner, for example, to scatter random dots over a limited range of eccentricities (from 5° to 8° in Suchow & Alvarez, 2011), to measure critical spacing in crowding experiments (at 3.5° and 7° in Turi & Burr, 2013), or to circularly distribute dots at a specific eccentricity (6.42° in Choi et al., 2014). Understanding the effect of eccentricity on motion silencing is important for making the connection between the awareness of object appearance and motion in peripheral vision. Given the large changes in receptive field (RF) characteristics with eccentricity, we felt that parametrically varying them might reveal something about the mechanism underlying silencing.

Human psychophysics

Methods

Observers

Fifteen University of Texas students served as naïve observers. They ranged in age from 20 to 33 years and had normal or corrected-to-normal vision. Six of the observers were female. This project was approved by the Institutional Review Board at The University of Texas at Austin.

Apparatus

The experiments were programmed using MATLAB and the Psychophysics Toolbox (Brainard, 1997). The Psychophysics Toolbox interfaced with an NVIDIA GeForce GTX 780 graphics card in a Windows 7 computer. The experiment was conducted using a 24-inch liquid crystal display (LCD; ASUS, Model VG248QE, Fremont, CA). The spatial resolution was 1,920 × 1,080, with a pixel density of 94.34 ppi. The LCD refreshed at 120 Hz and was illuminated by a light-emitting diode backlight. Response time was 1 ms. We measured the display with a V-lambda–corrected fast photocell (United Detector Technologies PIN-10AP) and confirmed that the display consistently and correctly presented single-frame stimuli and was additive over frames with no interaction (so that a three-frame stimulus, for example, was just a repeated longer version of a one-frame stimulus at a 120-Hz temporal frequency response). The viewing distance was approximately 57 cm.

Stimuli

We used stimuli similar to those of Turi and Burr (2013) in the eccentricity study. The original demonstration used 15 dots at one eccentricity; therefore, the angular spacing was $2\pi/15$. We propagate the same angular spacing to four eccentricities (4°, 7°, 10°, and 13°) by replicating and extending Turi and Burr's (2013) eccentricity range. The stimulus consisted of four concentric rings of dots at eccentricities of 4°, 7°, 10°, and 13° as shown in Figure 1, Supplementary Movies S1–S6, and http://live.ece.utexas.edu/research/motion_silencing/eccentricity.html. Four rings of dots were simultaneously present to minimize the influence of factors other than eccentricity on the motion-silencing illusion. For example, if only one ring at different eccentricities was used, two difficulties might occur. First, each ring might have a different dot spacing given the same number of dots across eccentricities. Different dot spacings may influence the strength of the motion-silencing illusion, as we reported in previous work (Choi et al., 2014). Second, increasing the number of dots to maintain the same dot spacing at larger eccentricity might induce a different density factor that could affect the overall results, as reported in Anstis and Ho (2014), in which the apparent speed of rotating dots was observed to increase with dot density. Hence, we used stimuli consisting of four concentric rings of dots having the same number of dots on each ring and flickered the dots of no more than one ring at a time.

A red fixation mark was used at center. The diameter of each dot was 0.92° visual angle. The initial luminance of each dot was chosen randomly from a uniformly distributed eight-bit gray scale ranging from "black" at the weakest intensity to "white" at the strongest. Once the presentation commenced, the luminance of each dot of a selected ring changed sinusoidally against a gray background. The luminances of the black dots, white dots, and the gray background were 0.92, 344.40, and 50.59 cd/m^2, respectively. The four rings of dots continuously rotated in either a clockwise or a counterclockwise direction; the direction was alternated between clockwise and counterclockwise (i.e., clockwise, counterclockwise, then clockwise and counterclockwise). We did this to minimize any direction-specific motion adaptation in the subjects. The rotational velocity of the rings was the instantaneous tangential speed of a dot as it followed its circular trajectory on the screen, which was expressed in terms of angular degree per second (angular degree/s). The range of rotational velocities was from 40 to 350 angular degree/s based on pilot data, and the initial velocity did not change during each trial. In each presentation, the dots on no more than one of the four rings changed in luminance, at a flicker frequency that was fixed at 1/4 Hz. The

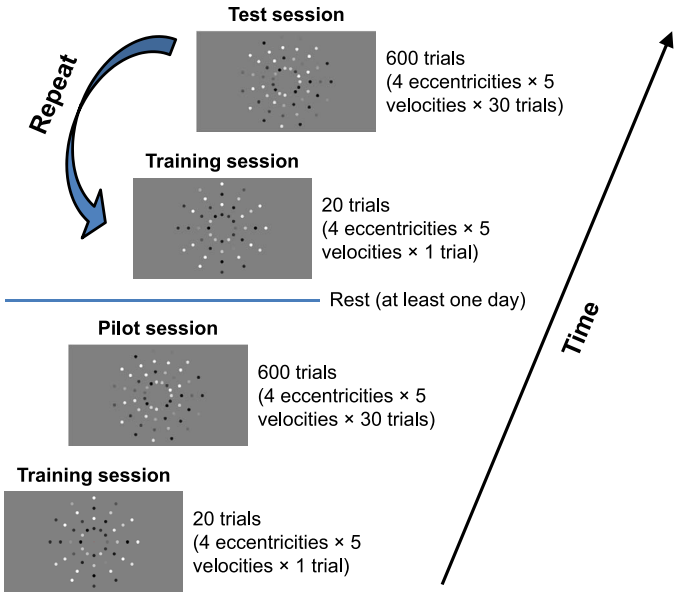

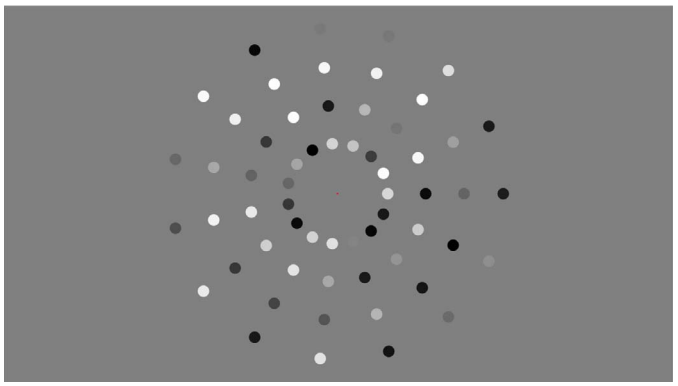

Figure 1. (a) Illustration of experimental setup. Prior to data collection for each test set, observers executed a short training session of 20 trials, in which the stimuli were similar to a real test but with different flicker frequency, velocity, eccentricity, and dot spacing. Observers first participated in a pilot session to find five stimulus velocities that were used in test sessions at eccentricities 4°, 7°, 10°, and 13°, then performed a series of test sessions for data collection. (b) Example of stimuli used in the human psychophysical experiment. Stimulus consisted of four concentric rings of dots at eccentricities 4°, 7°, 10°, and 13° in a regular array of uniform angular spacing $2\pi/15$, which rotated around a central fixation mark. Each dot was 0.92° visual angle in diameter. The luminance of each dot was chosen randomly from a range falling between black (0.92 cd/m^2) and white (344.40 cd/m^2) against a gray (50.59 cd/m^2) background. The four rings of dots continuously rotated together at a given velocity, whereas the dots on no more than one of the four rings changed in luminance with a sinusoidal variation of frequency 1/4 Hz.

dots in the other three rings remained at fixed luminances.

Design and procedure

Observers were asked to indicate whether or not the dots in any of four concentric rings were flickering (i.e., changing luminances), as distinct from the other dots whose luminances remained constant. During the experiments, the observers were asked to hold their gazes on a red central fixation mark.

The stimulus velocity was varied over five values at each eccentricity, where the particular velocities were chosen per observer to produce a good psychometric function based on pilot data (with *good* meaning spanning the ascending part of the function without unduly sampling the tails). For each stimulus velocity, 30 trials were executed, 15 of which presented flickering dots and the remaining 15 did not.

For each trial, a "yes/no" procedure was used, in which "yes" corresponded to "I think the dots are flickering" (because half the trials were catch trials, chance performance was 50%). Each stimulus was presented until observers made their judgment (average response time was approximately 3 to 5 s), and the following trial was automatically initiated after recording the response. To minimize the effects of observer fatigue and eye strain, the observers were required to rest for as long as needed (at least 2 min) after finishing every 100 trials. After completing the first set (four eccentricities $\times$ five velocities $\times$ 30 trials), each observer repeated the test set twice more, for a total of three sets ($4 \times 5 \times 30 \times 3$, or 1,800 total trials per observer). Observers had enough rest before executing the next set (e.g., 1 day). The order of all trials was randomized. Prior to data collection for each set, a short training exercise including 20 trials was conducted, which was similar to a real test but with a different flicker frequency, velocity, eccentricity, and dot spacing of the visual stimuli.

A pilot session was executed to find five stimulus velocities to be used in the test sessions at each eccentricity per observer using pilot data from a set of 600 trials (four eccentricities $\times$ five velocities $\times$ 30 trials). Table 1 shows the five pilot velocities and the variabilities of the velocities chosen across the observers on the actual test at eccentricities 4°, 7°, 10°, and 13°. After shifting five pilot velocities together by a unit of 10 angular degree/s, to obtain a good psychometric function, the changed velocities were chosen as the five velocities deployed in the actual test. When there was no velocity change from the pilot velocities, the result of a pilot session was used as the result of the first test set, and then each observer executed the test set twice more; otherwise, the observers executed three test sets with the changed velocities.

Eccentricity	Pilot velocity (angular degree/s)	Variability of the velocities chosen across the observers from pilot velocity
4°	70, 140, 210, 280, 350	0, +10, +20
7°	80, 140, 200, 260, 320	−20, −10, 0
10°	60, 110, 160, 210, 260	−30, −10, 0
13°	40, 80, 120, 160, 200	−20, 0, +10

Table 1. Pilot velocities and the variabilities of the velocities chosen across the observers on the actual test at eccentricities 4°, 7°, 10°, and 13°.

Results

Figure 2a shows psychometric curves (Weibull, 1951; Wichmann & Hill, 2001) as a function of velocity for an observer at eccentricities 4°, 7°, 10°, and 13°, respectively. The error bars using the binomial distribution with 68% confidence intervals are also shown. All observers executed the experiment in a similar manner. The velocity corresponding to a probability of detection equal to 0.75 (a thick, horizontal dashed line in Figure 2a) was chosen as the threshold velocity for motion silencing. As eccentricity increased, the psychometric curves shifted to the left, decreasing the threshold velocity for motion silencing, which indicates that motion silencing clearly depended on eccentricity.

Figure 2b shows the average of the threshold velocities for all observers as a function of log eccentricity when motion silencing occurred. Error bars are shown with 95% confidence intervals. The threshold velocity for motion silencing linearly decreased when log eccentricity increased. The average of the threshold velocities was 240.3, 165.0, 115.0, and 97.8 angular degree/s at eccentricities of 4°, 7°, 10°, and 13° (corresponding log eccentricities were 1.39, 1.95, 2.30, and 2.56), respectively. The slope of the least squares fit for the measured data from observers was approximately −124.59. The linear fit of the data is shown using a straight line, whereas 95% confidence intervals are shown using dashed lines in Figure 2b. The strong and consistent decrease of the threshold velocity suggests that there exists a significant effect of eccentricity on motion silencing.

Motion energy model

Methods

Stimuli

A total of 720 stimuli were created similar to those shown to the human observers (Figure 1). However, a wider range of velocities was used: four eccentricities (4°, 7°, 10°, and 13°) × 18 velocities (20, 40, . . . , 340, and 360 angular degree/s) × 10 times. In each trial, the luminances of dots were randomly selected, and the dots on exactly one of the four rings always changed in luminance while rotating in a clockwise direction.

Space-time diagram and spectral signatures of stimuli

To separately quantify collective motion and the local flicker frequency of the dots across eccentricity,

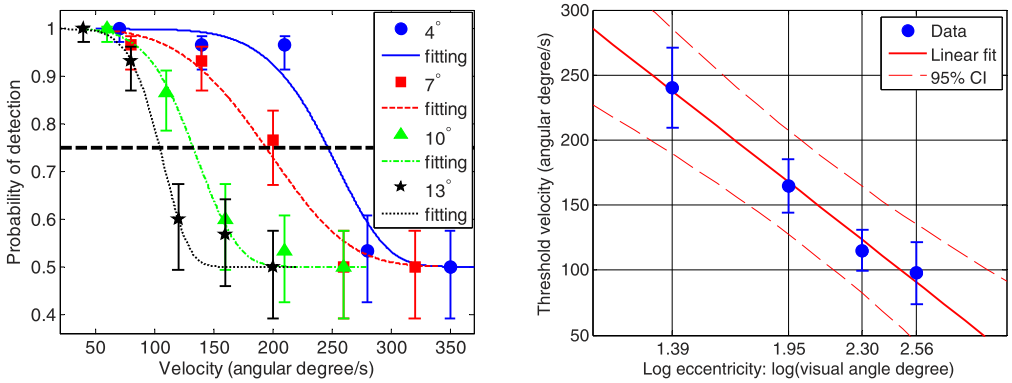

Figure 2. (a) Psychometric data fitted to the Weibull function of one observer to investigate the effect of eccentricity on motion silencing. The combined motion-flicker stimuli were shown at various velocities across eccentricities 4° (●), 7° (■), 10° (▲), and 13° (★). The velocity corresponding to a probability of detection equal to 0.75 (a thick, horizontal dashed line) was chosen as the threshold velocity for motion silencing. Error bars using the binomial distribution with 68% confidence intervals are shown. (b) The average of the threshold velocities for all observers as a function of log eccentricity when motion silencing occurs. Error bars are shown with 95% confidence intervals (CIs). A least-squares fit of the human data is shown with 95% CI together. The threshold velocity for motion silencing almost linearly decreased when log eccentricity increased.

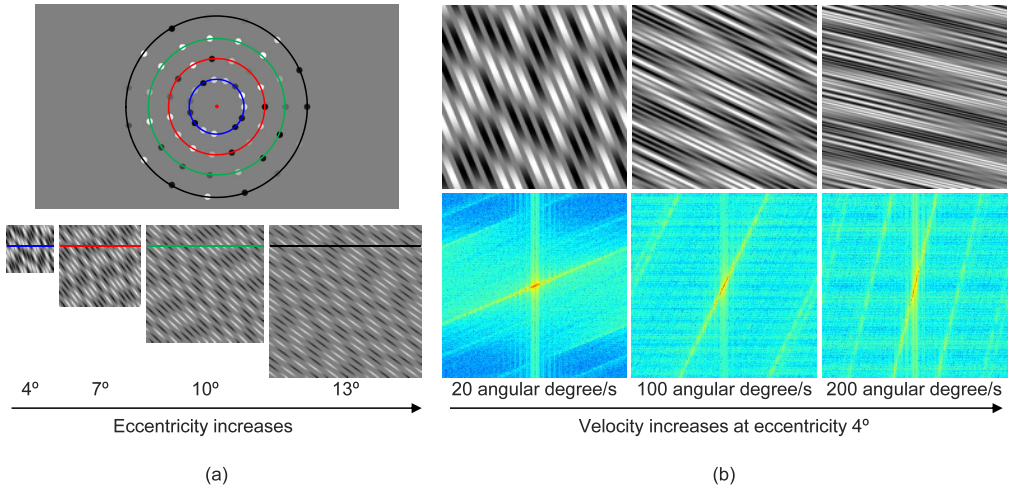

Figure 3. (a) Space-time diagram of stimuli. Top: Circles overlaid on dots shown in Figure 1 measure luminance along the ring at each eccentricity: *Note*: The red dot in the middle of this panel has been enlarged so as to display within the article. It does not represent the size used in the stimuli. Bottom: Space-time diagrams displayed as images under various eccentricities. The arrow on the bottom indicates the increase of eccentricity. (b) Spectral signatures of stimuli. Top: Space-time diagrams at specified velocities (20, 100, and 200 angular degree/s from left to right) and at eccentricity 4°. Bottom: The discrete Fourier transform (DFT) magnitudes (centered and logarithmically compressed to reveal the DFT structure) of space-time diagrams shown at the top. The arrow at the bottom indicates the increase of velocity. The energy levels of the spectral signatures are rendered from cool (low energy) to hot (high energy).

we first constructed a two-dimensional (2D) space-time diagram (indexed array) from the continuously moving stimuli and represented it as an image (Choi et al., 2014). As shown at the top of Figure 3a, we used a circle passing through the center of each dot in each ring of the visual stimuli to generate the 2D diagram (a circular trace). The luminance along the length/circumference of each ring was straightened into a horizontal row or vector starting at a fixed angle (0°) and continuing in a clockwise direction. These circular traces through the luminance changing dots constituted the rows of the space-time diagrams displayed in the bottom of Figure 3a. Uniformly sampling the luminance over time at 120 Hz generated additional rows, the stack of which constituted the space-time diagram. Thus, vertical columns of the space-time diagram contained temporal luminance variances at fixed spatial positions on a circle in the video.

The spectral signatures of the stimuli (bottom of Figure 3b) were created from the 2D space-time diagram (top of Figure 3b) using the discrete Fourier transform (DFT). The orientation of high-energy spectral signatures rendered in hot (red or yellow) consistently increased with respect to the horizontal when velocity increased (bottom of Figure 3b). The DFT of the space-time diagram of the stimulus was used as an input to a spatiotemporal filter-based energy model of the population responses of neurons in the primary visual cortex (V1).

Spatiotemporal filter-based energy model

We used a spatiotemporal filter model (Adelson & Bergen, 1985; T. I. Baker & Issa, 2005; Hubel & Wiesel, 1962; Mante & Carandini, 2005; Movshon, Thompson, & Tolhurst, 1978; Rasch, Chen, Wu, Lu, & Roe, 2013; Watson & Ahumada, 1985) of the responses of neurons in V1 as a function of eccentricity. In this model, the shape of a filter is identified as the RF of a neuron. This model assumes that the firing rate of a single neuron can be expressed as the filtered version of the spectral signatures falling within its RF. The population responses of neurons in V1 can be modeled as the sum of the squares of quadrature-pair Gabor filter outputs. We implemented such a Gabor filtering model similar to spatial models (Bovik, Clark, & Geisler, 1990; Clark & Bovik, 1989; Daugman, 1985; Jones & Palmer, 1987) but also modeling the spatiotemporal energy capturing mechanism in Adelson and Bergen (1985). Gabor RFs were tuned to peak spatial and temporal frequencies and bandwidths across eccentricity. Because the size of the space-time diagram of stimuli varied with eccentricity as shown in Figure 3a, the summed product of each Gabor filter and the 2D DFT of the space-time diagram was divided by the size of the space-time diagram.

RF parameters of an energy model

We implemented the RFs of an energy model based on measured spatiotemporal selectivity of V1 neurons

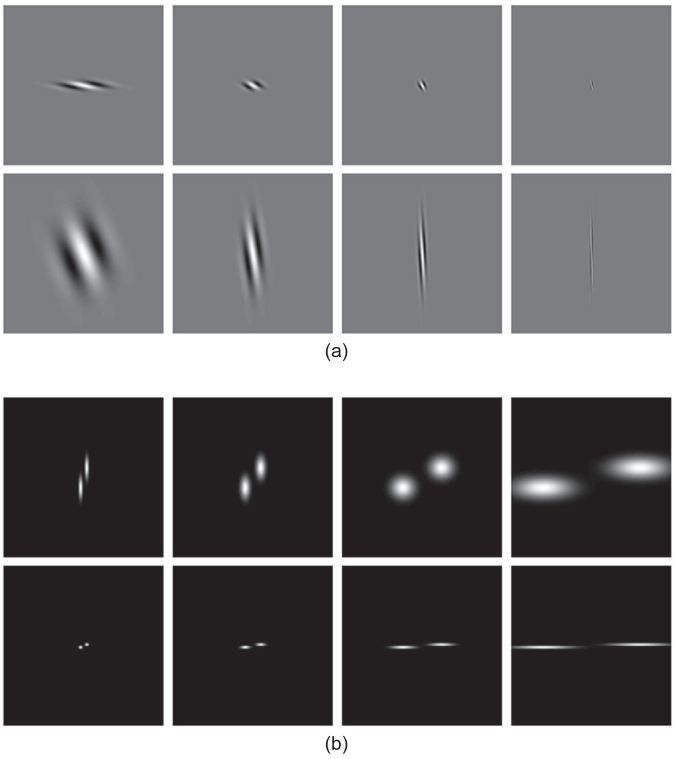

Figure 4. Examples of spatiotemporal Gabor functions matched to the parameters of receptive fields (RFs) at eccentricity 4° from V1 in macaques. (a) Cosine Gabor RFs in the space (horizontal axis)–time (vertical axis) domain. (b) Spatiotemporal profiles of Gabor RFs corresponding to (a) in the frequency domain. The center is zero spatiotemporal frequency. The peak spatial frequencies were 0.3529, 0.8812, 2.2, and 5.4927 cpd from left to right, with a spatial bandwidth of 1.32 octaves. The peak temporal frequencies were 3.7 and 0.4957 Hz from top to bottom, with a temporal bandwidth of 2.9 octaves. The Gabor functions were centered and magnified for rendering in figures.

in macaque monkeys (De Valois, Albrecht, & Thorell, 1982; Foster, Gaska, Nagler, & Pollen, 1985; Schiller, Finlay, & Volman, 1976; Tootell, Silverman, Hamilton, Switkes, & De Valois, 1988; Xu, Anderson, & Casagrande, 2007) and humans (Henriksson, Nurminen, Hyvarinen, & Vanni, 2008; Sasaki et al., 2001; Singh, Smith, & Greenlee, 2000). Because there are differences in the measurements of the average peak spatial frequencies across eccentricity between macaques and humans, we tested the RF parameters from both macaques (Test 1) and from humans (Test 2). In macaques, the average preferred peak spatial frequencies was 2.2 cycles per degree (cpd) at parafoveal (De Valois et al., 1982; Foster et al., 1985) and approximately 0.5 cpd at eccentricity of 20° (Pack, Conway, Born, & Livingstone, 2006), whereas the median bandwidth was 1.32 octaves. In humans, the average preferred peak spatial frequencies measured by functional magnetic resonance imaging was 1.2, 0.68, 0.46, 0.40, and 0.18 cpd at eccentricities 1.7°, 4.7°, 6.3°, 9°, and 19°, respectively (Henriksson et al., 2008). The average preferred peak temporal frequency was 3.7 Hz, whereas the average temporal bandwidth was 2.9 octaves at parafoveal in macaques (Foster et al., 1985). We used Foster et al.'s measurements for both Test 1 (macaques) and Test 2 (humans) because Foster et al.'s results were consistently found in Kelly's (1979) psychophysical data (peak temporal frequency between 3 and 5 Hz; peak 3.2 Hz) and Watson and Turano's (1995) results (the optimal motion stimulus found at 5 Hz) as well as being used widely in the literature, although some studies reported an average peak temporal frequency of 10 Hz (Anderson & Burr, 1985; Hawken, Shapley, & Grosof, 1996).

The population of neurons in our experiments covered four peak spatial frequencies and four peak temporal frequencies. The peak spatial frequencies were 0.3529, 0.8812, 2.2, and 5.4927 cpd in Test 1 (macaques) and 0.115, 0.287, 0.7166, and 1.7892 cpd in Test 2 (humans), respectively, at eccentricity 4° with a constant spatial bandwidth of 1.32 octaves. The peak temporal frequencies were 0.0089, 0.0664, 0.4957, and 3.7 Hz with a constant temporal bandwidth of 2.9 octaves. Figure 4 shows examples of the Gabor functions used at 4° eccentricity in Test 1.

The spatial and temporal tuning bandwidths were similar across a large range of eccentricities on an octave scale (De Valois et al., 1982; Foster et al., 1985; Kelly, 1984; Snowden & Hess, 1992; Virsu, Rovamo, Laurinen, & Nasanen, 1982; Yu et al., 2010). The peak temporal frequency does not change dramatically with respect to eccentricity on an octave scale. However, as eccentricity increases, the peak spatial frequency decreases, shifting the populations of peak spatial frequency neurons away from high spatial frequencies (De Valois et al., 1982; Foster et al., 1985; Henriksson et al., 2008; Ikeda & Wright, 1975; Movshon et al., 1978; Rovamo, Virsu, & Nasanen, 1978; Sasaki et al., 2001; Schiller et al., 1976; Tootell et al., 1988; Xu et al., 2007). Thus, we applied the peak spatial frequencies of 2.2, 1.8813, 1.5625, and 1.2438 cpd in Test 1 (macaques) and 0.7166, 0.469, 0.3485, and 0.2773 cpd in Test 2 (humans) at eccentricities 4°, 7°, 10°, and 13°, respectively, by least square fits of the known measurements. The magnitude of the Gabor RF kernel was normalized for each neuron, such that the response elicited by the stimuli was the same across the neurons. Figure 5 shows the frequency responses of all Gabor-energy filters used in Test 1 across eccentricity. It may be observed that the peak spatial frequency of the neuronal populations are shifted away from high spatial frequencies with increasing eccentricity and that the spatial frequency bandwidths are much narrower for neurons tuned to low spatial frequencies (on a linear scale).

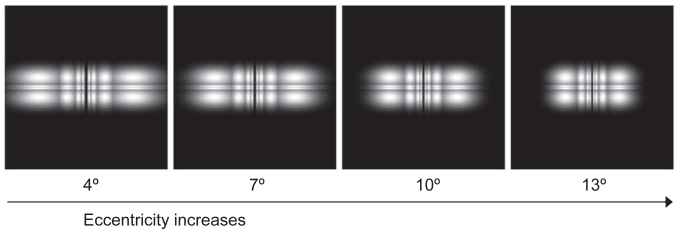

Figure 5. Spatiotemporal profile of the Gabor-energy filters across eccentricity. The filters covered four peak spatial frequencies and four peak temporal frequencies, where the parameters of the receptive fields (RFs) were matched to V1 in macaques (Test 1): The peak spatial frequencies of the third subband at eccentricities 4°, 7°, 10°, and 13° were 2.2, 1.8813, 1.5625, and 1.2438 cpd, respectively, with a constant spatial bandwidth of 1.32 octaves. The peak spatial frequencies of neuronal populations were shifted away from high spatial frequencies with increasing eccentricity. The peak temporal frequencies were 0.0089, 0.0664, 0.4957, and 3.7 Hz with a constant temporal bandwidth of 2.9 octaves. The center is zero spatiotemporal frequency. Energy levels are shown from black (low) to white (high). The Gabor functions were centered and magnified for visually distinctive rendering.

Results

Test 1 and Test 2 in the motion energy model assessed whether a spatiotemporal filter-based energy model could be used to explain the effect of eccentricity on motion silencing. If there is a constant threshold energy for motion silencing, the threshold velocities of the energy model should consistently match the threshold velocities obtained from the human psychophysical experiment. Two sets of parameters derived from published research (Test 1: measurements of De Valois et al., 1982, and Pack et al., 2006, from macaque V1; Test 2: measurements of Henriksson et al., 2008, from human V1) were used to implement Gabor RFs across eccentricity.

The population responses of Gabor RFs are shown in Figure 6a and 6c from a total of 720 stimuli at diverse velocities across eccentricities 4°, 7°, 10°, and 13°. As motion velocity increases, the population responses consistently decrease for all eccentricities, even though the specific values vary somewhat between Test 1 and Test 2, especially for velocities smaller than 60 angular degree/s.

The threshold velocity of the energy model was predicted by assuming that there is a single constant threshold energy (i.e., the population response) for motion silencing for the set of RF parameters in Test 1 (measurements of De Valois et al., 1982, and Pack et al., 2006, from macaque V1) and Test 2 (measurements of Henriksson et al., 2008, from human V1), respectively. Specifically, the threshold energy for motion silencing was first assumed at each eccentricity to be the population response at the threshold velocities obtained from the human psychophysics (i.e., 240.3, 165.0, 115.0, and 97.8 angular degree/s at eccentricities 4°, 7°, 10°, and 13°, respectively, as shown in Figure 2) using the least-squares fitting curve depicted in Figures 6a and 6c. Then, the threshold energy assumed at each eccentricity (e.g., 5.43×10^4, 5.35×10^4, 6.66×10^4, and 6.41×10^4 at eccentricities 4°, 7°, 10°, and 13°, respectively, in Test 1) was averaged to determine one constant threshold energy (e.g., 5.97×10^4 in Test 1). Next, the velocities corresponding to the constant threshold energy (e.g., 5.97×10^4 in Test 1) were chosen as the threshold velocities of the energy model across eccentricities. The mean of the predicted threshold velocities from a total of 720 stimuli were 224.4, 154.3, 123.4, and 102.6 angular degree/s and 233.9, 159.7, 122.2, and 98.3 angular degree/s at eccentricities 4°, 7°, 10°, and 13° in Test 1 and Test 2, respectively, as shown in Figure 6b and 6d.

To assess whether the threshold velocities observed in the human experiment and those seen in the energy model are related, we plotted all data together in one plot and tested for statistically significant differences using the Kruskal-Wallis test. Figure 7 shows the results. The threshold velocities at the same log eccentricity among the human experiment, Test 1, and Test 2 of the energy model are not significantly different across all eccentricities ($p = 0.3844$, 0.6484, 0.0536, and 0.1122 at eccentricities 4°, 7°, 10°, and 13°, respectively), and the threshold velocity for motion silencing almost linearly decreases as a function of log eccentricity. These results indicate that the threshold velocities of the human psychophysical experiment and the energy model stem from the same statistical distribution. The strong matches of the threshold velocities between the human experiment and the model tests imply that the spatiotemporal selectivity of V1 neurons across eccentricity should play an important role in the energy model describing the dependence of motion silencing on eccentricity.

Discussion

The results of this study strongly suggest that eccentricity significantly affects motion silencing. The threshold velocity for motion silencing almost linearly decreases as a function of log eccentricity, where the mean slope was approximately −124.59 (Figure 2b). The human psychophysical results from this study provide evidence that the dependence of silencing on motion (Suchow & Alvarez, 2011) varies with eccentricity: The average of the threshold velocities was 240.3, 165.0, 115.0, and 97.8 angular degree/s at eccentricities 4°, 7°, 10°, and 13°, respectively, at $2\pi/15$

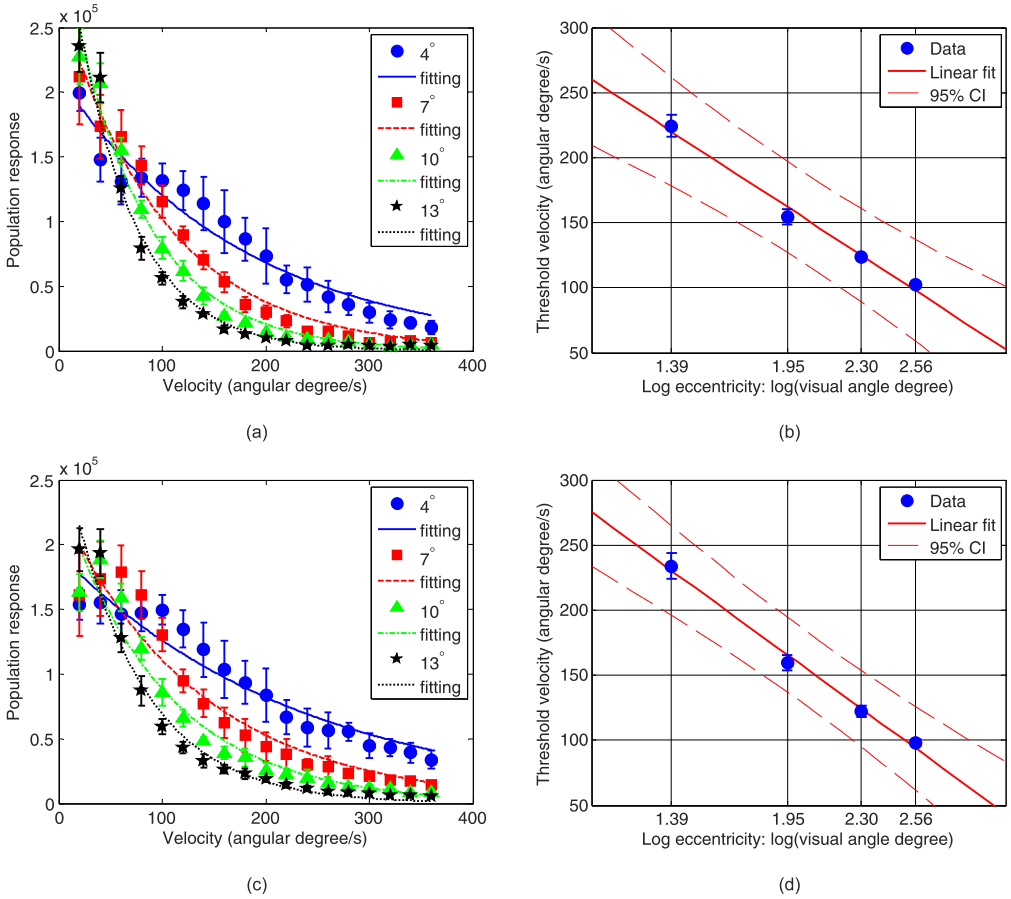

Figure 6. Population responses seen in the spatiotemporal energy model from a total of 720 combined motion-flicker stimuli across eccentricities 4° (●), 7° (■), 10° (▲), and 13° (★) in Test 1 and Test 2. The receptive field (RF) parameters that were used derive from the measurements of (a) De Valois et al. (1982) and Pack et al. (2006) from V1 of macaques in Test 1 and of (c) Henriksson et al. (2008) from V1 of humans in Test 2. Error bars indicating 95% confidence intervals are included. Threshold velocities for motion silencing seen in the energy model in Test 1 and in Test 2 are shown in (b) and (d), respectively, and were achieved using the population responses in (a) and (c).

angular dot spacing and 1/4-Hz dot flicker frequency. Although the specific threshold velocities might be influenced when the flicker frequency or dot spacing changes as reported in the literature (Choi et al., 2014; Peirce, 2013; Turi & Burr, 2013), the effect of eccentricity on motion silencing might also be similar.

The spatiotemporal energy model offers a plausible and meaningful explanation of why eccentricity affects motion silencing in peripheral vision. The strong statistical matches between the measured threshold velocities for motion silencing from the human experiment and the predicted threshold velocities from the energy model (Figure 7) indicate that the spatiotemporal selectivity of V1 neurons across eccentricity provides a compelling functional account of the dependence of motion silencing on eccentricity. We investigated the population responses of V1 neurons using the energy model by implementing Gabor functions mimicking the spatiotemporal selectivity of neurons in V1 so that the model responses were consistent with the population of RFs implicated with flicker visibility over a plausible range of spatiotemporal frequencies.

In V1, when eccentricity increases, the peak spatial frequency responses of neuronal populations are shifted away from high spatial frequencies (De Valois et al., 1982; Foster et al., 1985; Henriksson et al., 2008; Ikeda & Wright, 1975; Movshon et al., 1978; Rovamo et al., 1978; Sasaki et al., 2001; Schiller et al., 1976; Xu et al., 2007), so a sample at large eccentricity does not include cells tuned to high spatial frequencies. On the other hand, the bandwidths of spatial tuning are remarkably similar across the range of eccentricities on an octave scale (Anderson & Burr, 1985; De Valois et al., 1982) and significantly correlated with peak spatial frequency (G. E. Baker, Thompson, Krug, Smyth, & Tolhurst, 1998; De Valois et al., 1982; Movshon et al., 1978; Tolhurst & Thompson, 1981). Hence, the distributions of RFs in peripheral vision are similar to those of central vision but shifted along peak spatial

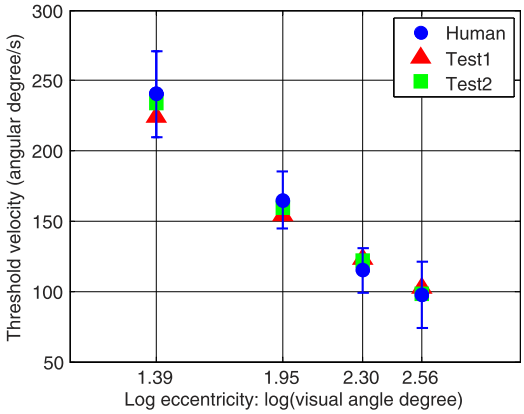

Figure 7. Comparison of the threshold velocities obtained from the human experiment (Figure 2b) and the energy model (Test 1, Figure 6b; Test 2, Figure 6d). The horizontal axis indicates log eccentricity, whereas the vertical axis shows threshold velocity (angular degree/s). The threshold velocities at the same log eccentricity among the human experiment, Test 1, and Test 2 of the energy model are not significantly different across all eccentricities, where $p = 0.3844$, 0.6484, 0.0536, and 0.1122 at eccentricities 4°, 7°, 10°, and 13°, respectively, in the Kruskal-Wallis test.

frequency, which narrows the total range of spatial frequency peaks (De Valois et al., 1982; Tolhurst & Thompson, 1981). Note that on a linear scale, the spatial frequency bandwidths are much narrower for cells tuned to low spatial frequencies than those tuned to high frequencies (De Valois et al., 1982), as shown in Figures 4 and 5.

The distributions of the peak temporal frequency and temporal bandwidth do not change dramatically with respect to eccentricity on an octave scale, which is consistent with human psychophysical data showing that temporal contrast sensitivity is fairly constant across a wide range of eccentricities (Foster et al., 1985; Kelly, 1984; Snowden & Hess, 1992; Virsu et al., 1982; Yu et al., 2010).

Regarding the spatiotemporal tuning and interactions of neurons in V1, the optimal temporal frequency was not correlated with optimal spatial frequency across eccentricities (Foster et al., 1985; Holub & Morton-Gibson, 1981; Ikeda & Wright, 1975; Kelly, 1984; Virsu et al., 1982; Yu et al., 2010). It is commonly assumed that spatial and temporal tuning of V1 neurons do not interact each other, so spatiotemporal tuning surfaces can be modeled as the product of spatial and temporal tuning curves, each measured independently. Kelly (1984) suggested that at eccentricities out to 12°, the entire threshold spatiotemporal surface is merely translated toward lower spatial frequency with increasing eccentricity. Therefore, as eccentricity increases, the spectral signatures of the combined motion-flicker signal fall outside the response regions of neurons that elicit large responses, thereby reducing the total population response in a spatiotemporal filter-based energy model, consequently leading to declining flicker visibility in peripheral vision.

Why does eccentricity influence the degree of motion silencing? Is it just a side effect of the shift of the population tuning away from high spatial frequencies or a compromise between motion perception and change perception? Neurons representing peripheral vision are essential for visual performance such as defensive reaction, balance, and locomotion as well as survival, which demand accurate *perception* of motion rather than necessarily recognizing detail objects or their temporal changes at relatively short latencies (Thompson, Hansen, Hess, & Troje, 2007; Yu et al., 2010). Thus, evolution may have kept motion perception in the peripheral visual field but may have not retained high-frequency change perception among the populations of peripheral neurons. This might be related to observations that peripheral vision is sensitive to higher speeds (Orban, Kennedy, & Bullier, 1986), reflecting the distribution of retinal image speed sensing of natural environments. Human psychophysical studies have also demonstrated that central vision is most sensitive to speeds slower than 1°/s, whereas at 40° eccentricity, the peak sensitivity value is shifted approximately to 30°/s (Kelly, 1984; McKee & Nakayama, 1984).

One cannot exclude the possibility that the effect of eccentricity on motion silencing also includes RF sizes' relationship with eccentricity. The average size of RFs in foveal V1 is as small as a 1 to 2 min of arc and as large as 60 min of arc at eccentricity 20° and increasing with increasing eccentricity (Dow, Snyder, Vautin, & Bauer, 1981; Dumoulin & Wandell, 2008). Neurons at great eccentricities tolerate large stimulus jumps using a large RF size, preferring lower spatial frequencies (De Valois et al., 1982) and higher velocities (Orban et al., 1986) to perceive crucial motion signals. Accurate representations of motion, including speed, may benefit from integration over a large spatial aperture (Grzywacz & Yuille, 1990).

In the motion energy model, we tested two sets of RF parameters on the V1 in macaques (Test 1) and in humans (Test 2), as shown in Figure 6. On average, the spatial tuning curves of V1 neurons shift toward lower spatial frequencies as eccentricity increases (De Valois et al., 1982; Foster et al., 1985; Henriksson et al., 2008; Movshon et al., 1978; Schiller et al., 1976; Tootell et al., 1988; Xu et al., 2007). However, there exists considerable scatter of the peak spatial frequencies (De Valois et al., 1982; Foster et al., 1985; Henriksson et al., 2008; Pack et al., 2006) at any given eccentricity. In addition, the eccentricities used when making the experimental measurements varied (e.g., foveal: 0°–1.5°, parafoveal:

3°–5° in De Valois et al., 1982; foveal: 0.5°–1.0°, parafoveal: 2°–5° in Foster et al., 1985; approximately 0°–25° in Pack et al., 2006; 1.7°–19° in Henriksson et al., 2008), so we used least squares fitting to estimate the peak spatial frequency at eccentricities 4°, 7°, 10°, and 13° from the known average peak spatial frequencies. Although the population responses in our tests varied somewhat when predicting the threshold velocities on silencing for each RF parameter set in both macaques and humans, we reached similar conclusions from the well-matched, overlapped data (Figure 7) and the corresponding statistical analysis.

The results we have described are of interest to vision science because they confirm and extend our prior understanding of motion silencing (Choi, Bovik, & Cormack, 2012; Choi et al., 2014; Peirce, 2013; Suchow & Alvarez, 2011; Turi & Burr, 2013) and its underlying mechanisms. In particular, we believe that being able to explain the effects of eccentricity using our "back-pocket" V1 model using no free parameters strongly solidifies our contention that the motion-silencing illusion falls out of known mechanisms of early visual processing. To wit, a primary if not only way in which early visual processing is heterogeneous is in its variation as a function of eccentricity. We therefore think that a crucial test of our thesis was indeed to explicitly manipulate eccentricity.

These results are also important as they provide the groundwork for specific perception-based video-processing applications to yield quantitative models of perceived local flicker in less-than-perfect digital videos (such as compressed television signals) and to explain one mode of temporal visual masking of video flicker distortions. Specifically, this extension not only reveals a lawful relationship between a threshold velocity and log eccentricity when motion silencing occurs but also proposes a plausible explanation of why motion silencing decreases when eccentricity increases in peripheral vision, using a spatiotemporal energy model (Adelson & Bergen, 1985). For perceptual applications on digital videos, the motion-silencing phenomenon has been a basis for understanding the influence of motion on the visibility of flicker distortions in naturalistic videos (Choi, Cormack, & Bovik, 2013, 2015a, 2015b) and for developing a perceptual flicker visibility prediction model (Choi & Bovik, 2016b) as well as a new video quality assessment method (Choi & Bovik, 2016a). We believe that a better understanding of temporal flicker masking will play an increasingly important role in modern models of temporal vision and objective video quality assessment.

Turi and Burr's (2013) work showed that the strength of the motion-silencing illusion increases with eccentricity. However, the task and purpose of their human experiments were different. Turi and Burr used two eccentricities (3.5° and 7°) to try to explain the motion-silencing illusion in terms of crowding. They found that silencing depends on the target-flanker spacing with a critical spacing of about half eccentricity, following Bouma's law (Bouma, 1970). Their experimental results contributed to our understanding of the eccentricity effect of motion silencing. Our results go beyond this by detailing a quantitative monotonic power-law relationship (a straight line on the log-linear plot in Figures 2, 6, and 7), over four eccentricities (4°, 7°, 10°, and 13°). In addition, our cortical model (with no free parameters) captures the data quantitatively as well as qualitatively. Based on our human psychophysical data and using a spatiotemporal energy model of V1 neurons, we proposed a plausible quantitative explanation of the underlying effect of eccentricity on motion silencing. We believe that this work embodies significant evidence that the motion-silencing illusion simply falls out of what we already know about early cortical processing.

Because the early retinotopic areas exhibit approximately separable tuning of spatial and temporal frequencies (Foster et al., 1985; Priebe, Lisberger, & Movshon, 2006), we implemented a spatiotemporal filter-based energy model (Adelson & Bergen, 1985) using classical separable Gabor functions (Bovik et al., 1990; Daugman, 1985; Jones & Palmer, 1987). However, as Adelson and Bergen (1985) reported, the temporal response can be physiologically better approximated by other linear filter forms such as causal gamma-modulated sinusoids (Watson & Ahumada, 1985). In addition, it might prove productive to include nonlinear constant gain control mechanisms such as divisive normalization (Heeger, 1992) to more completely model the overall responses of V1 neurons.

In summary, the intention of this study was to determine the degree to which motion silencing consistently depends on eccentricity and whether a quantitative spatiotemporal filter-based energy model could explain the dependence of motion silencing on eccentricity. We suggested the simple explanation that as eccentricity increases, the combined motion-flicker signal eventually falls outside of the narrower frequency passbands of peripheral RFs, although peripheral crowding (Turi & Burr, 2013) might also supply an explanation of reduced peripheral flicker visibility.

Keywords: motion silencing, eccentricity, spatiotemporal energy, peripheral vision, flicker

Acknowledgments

This work was supported by Intel and Cisco Corporations under the VAWN program and by the

National Science Foundation under Grants IIS-0917175 and IIS-1116656.

Commercial relationships: none.
Corresponding author: Alan C. Bovik.
Email: bovik@ece.utexas.edu.
Address: Department of Electrical and Computer Engineering, The University of Texas at Austin, Austin, TX, USA.

References

Adelson, E. H., & Bergen, J. R. (1985). Spatiotemporal energy models for the perception of motion. *Journal of the Optical Society of America A*, *2*, 284–299.

Anderson, S. J., & Burr, D. C. (1985). Spatial and temporal selectivity of the human motion detection system. *Vision Research*, *25*, 1147–1154.

Anstis, S., & Ho, A. (2014). Apparent speed of a rotating disk varies with texture density. *Journal of Vision*, *14*(10):1333, doi:10.1167/14.10.1333. [Abstract]

Baker, G. E., Thompson, I. D., Krug, K., Smyth, D., & Tolhurst, D. J. (1998). Spatial-frequency tuning and geniculocortical projections in the visual cortex (areas 17 and 18) of the pigmented ferret. *European Journal of Neuroscience*, *10*, 2657–2668.

Baker, T. I., & Issa, N. P. (2005). Cortical maps of separable tuning properties predict population responses to complex visual stimuli. *Journal of Neurophysiology*, *94*, 775–787.

Bouma, H. (1970). Interaction effects in parafoveal letter recognition. *Nature*, *226*, 177–178.

Bovik, A. C., Clark, M., & Geisler, W. S. (1990). Multichannel texture analysis using localized spatial filters. *IEEE Transactions on Pattern Analysis and Machine Intelligence*, *12*, 55–73.

Brainard, D. H. (1997). The Psychophysics Toolbox. *Spatial Vision*, *10*, 433–436.

Choi, L. K., & Bovik, A. C. (2016a). Flicker sensitive motion tuned video quality assessment. *IEEE Southwest Symposium on Image Analysis and Interpretation* (*SSIAI*) 29–32.

Choi, L. K., & Bovik, A. C. (2016b).Perceptual flicker visibility prediction model. *IS&T Human Vision and Electronic Imaging*, (*HVEI*), *108*, 1–6.

Choi, L. K., Bovik, A. C., & Cormack, L. K. (2012). A flicker detector model of the motion silencing illusion. *Journal of Vision*, *12*(9): 777, doi:10.1167/12.9.777. [Abstract]

Choi, L. K., Bovik, A. C., & Cormack, L. K. (2014). Spatiotemporal flicker detector model of motion silencing. *Perception*, *43*, 1286–1302.

Choi, L. K., Cormack, L. K., & Bovik, A. C. (2013). On the visibility of flicker distortions in naturalistic videos. *IEEE International Workshop on Quality of Multimedia Experience*, (*QoMEX*), 164–169.

Choi, L. K., Cormack, L. K., & Bovik, A. C. (2015a). Eccentricity effect of motion silencing on naturalistic videos. *IEEE Global Conference on Signal and Information Processing*, (*GlobalSIP*), 1190–1194.

Choi, L. K., Cormack, L. K., & Bovik, A. C. (2015b). Motion silencing of flicker distortions on naturalistic videos. *Signal Processing: Image Communication*, *39*, 328–341.

Clark, M., & Bovik, A. C. (1989). Experiments in segmenting text on patterns using localized spatial filters. *Pattern Recognition*, *22*, 707–717.

Daugman, J. G. (1985). Uncertainty relation for resolution in space, spatial frequency, and orientation optimized by two-dimensional visual cortical filters. *Journal of the Optical Society of America A*, *2*, 1160–1169.

De Valois, R. L., Albrecht, D. G., & Thorell, L. G. (1982). Spatial frequency selectivity of cells in macaque visual cortex. *Vision Research*, *22*, 545–559.

Dow, B. M., Snyder, A. Z., Vautin, R. G., & Bauer, R. (1981). Magnification factor and receptive field size in foveal striate cortex of the monkey. *Experimental Brain Research*, *44*, 213–228.

Dumoulin, S. O., & Wandell, B. A. (2008). Population receptive field estimates in human visual cortex. *Neuroimage*, *39*, 647–660.

Foster, K. H., Gaska, J. P., Nagler, M., & Pollen, D. A. (1985). Spatial and temporal frequency selectivity of neurons in visual cortical areas V1 and V2 of the macaque monkey. *Journal of Physiology*, *365*, 331–363.

Grzywacz, N. M., & Yuille, A. L. (1990). A model for the estimate of local image velocity by cells in the visual cortex, *Proceedings of the Royal Society of London. Series B: Biological Sciences*, *239*, 129–161.

Hawken, M. J., Shapley, R. M., & Grosof, D. H. (1996). Temporal-frequency selectivity in monkey visual cortex. *Visual Neuroscience*, *13*, 477–492.

Heeger, D. J. (1992). Normalization of cell responses in cat striate cortex. *Visual Neuroscience*, *9*, 181–197.

Henriksson, L., Nurminen, L., Hyvarinen, A., & Vanni, S. (2008). Spatial frequency tuning in human retinotopic visual areas. *Journal of Vision*, *8*(10):5, 1–13, doi:10.1167/8.10.5. [PubMed] [Article]

Holub, R. A., & Morton-Gibson, M. A. R. Y. (1981). Response of visual cortical neurons of the cat to moving sinusoidal gratings: Response-contrast functions and spatiotemporal interactions. *Journal of Neurophysiology*, *46*, 1244–1259.

Hubel, D. H., & Wiesel, T. N. (1962). Receptive fields, binocular interaction and functional architecture in the cat's visual cortex. *Journal of Physiology*, *160*, 106–154.

Ikeda, H., & Wright, M. J. (1975). Spatial and temporal properties of 'sustained' and 'transient' neurons in area 17 of the cat's visual cortex. *Experimental Brain Research*, *22*, 363–383.

Jones, J. P., & Palmer, L. A. (1987). An evaluation of the two-dimensional Gabor filter model of simple receptive fields in cat striate cortex. *Journal of Neurophysiology*, *58*, 1233–1258.

Kelly, D. H. (1979). Motion and vision. II. Stabilized spatio-temporal threshold surface. *Journal of the Optical Society of America A*, *69*, 1340–1349.

Kelly, D. H. (1984). Retinal inhomogeneity. I. Spatiotemporal contrast sensitivity. *Journal of the Optical Society of America A, Optics and Image Science*, *1*, 107–113.

Mante, V., & Carandini, M. (2005). Mapping of stimulus energy in primary visual cortex. *Journal of Neurophysiology*, *94*, 788–798.

McKee, S. P., & Nakayama, K. (1984). The detection of motion in the peripheral visual field. *Vision Research*, *24*, 25–32.

Movshon, J. A., Thompson, I. D., & Tolhurst, D. J. (1978). Spatial and temporal contrast sensitivity of neurons in areas 17 and 18 of the cat's visual cortex. *Journal of Physiology*, *283*, 101–120.

Orban, G. A., Kennedy, H., & Bullier, J. (1986). Velocity sensitivity and direction selectivity of neurons in areas V1 and V2 of the monkey: influence of eccentricity. *Journal of Neurophysiology*, *56*, 462–480.

Pack, C. C., Conway, B. R., Born, R. T., & Livingstone, M. S. (2006). Spatiotemporal structure of nonlinear subunits in macaque visual cortex. *Journal of Neuroscience*, *26*, 893–907.

Peirce, J. W. (2013). Is it just motion that silences awareness of other visual change? *Journal of Vision*, *13*(7):17, 1–10, doi:10.1167/13.7.17. [PubMed] [Article]

Priebe, N. J., Lisberger, S. G., & Movshon, J. A. (2006). Tuning for spatiotemporal frequency and speed in directionally selective neurons of macaque striate cortex. *Journal of Neuroscience*, *26*, 2941–2950.

Rasch, M. J., Chen, M., Wu, S., Lu, H. D., & Roe, A. W. (2013). Quantitative inference of population response properties across eccentricity from motion-induced maps in macaque V1. *Journal of Neurophysiology*, *109*, 1233–1249.

Rovamo, J., Virsu, V., & Nasanen, R. (1978). Cortical magnification factor predicts the photopic contrast sensitivity of peripheral vision. *Nature*, *271*, 54–56.

Sasaki, Y., Hadjikhani, N., Fischl, B., Liu, A. K., Marrett, S., & Dale, A. M., & Tootell, R. B. H. (2001). Local and global attention are mapped retinotopically in human occipital cortex. *Proceedings of the National Academy of Sciences, USA*, *98*, 2077–2082.

Schiller, P. H., Finlay, B. L., & Volman, S. F. (1976). Quantitative studies of single-cell properties in monkey striate cortex. III. Spatial frequency. *Journal of Neurophysiology*, *39*, 1334–1351.

Singh, K. D., Smith, A. T., & Greenlee, M. W. (2000). Spatiotemporal frequency and direction sensitivities of human visual areas measured using fMRI. *Neuroimage*, *12*, 550–564.

Snowden, R. J., & Hess, R. F. (1992). Temporal frequency filters in the human peripheral visual field. *Vision Research*, *32*, 61–72.

Suchow, J. W., & Alvarez, G. A. (2011). Motion silences awareness of visual change. *Current Biology*, *21*, 140–143.

Thompson, B., Hansen, B. C., Hess, R. F., & Troje, N. F. (2007). Peripheral vision: Good for biological motion, bad for signal noise segregation? *Journal of Vision*, *7*(10):12, 1–7, doi:10.1167/7.10.12. [PubMed] [Article]

Tolhurst, D. J., & Thompson, I. D. (1981). On the variety of spatial frequency selectivities shown by neurons in area 17 of the cat. *Proceedings of the Royal Society of London. Series B. Biological Sciences*, *213*, 183–199.

Tootell, R. B., Silverman, M. S., Hamilton, S. L., Switkes, E., & De Valois, R. L. (1988). Functional anatomy of macaque striate cortex: V. Spatial frequency. *Journal of Neuroscience*, *8*, 1610–1624.

Turi, M., & Burr, D. (2013). The "motion silencing" illusion results from global motion and crowding. *Journal of Vision*, *13*(5):14, 1–7, doi:10.1167/13.5.14. [PubMed] [Article]

Virsu, V., Rovamo, J., Laurinen, P., & Nasanen, R. (1982). Temporal contrast sensitivity and cortical magnification. *Vision Research*, *22*, 1211–1217.

Watson, A. B., & Ahumada, A. J. Jr. (1985). Model of human visual-motion sensing. *Journal of the*

Optical Society of America A, Optics and Image Science, *2*, 322–341.

Watson, A. B., & Turano, K. (1995). The optimal motion stimulus. *Vision Research*, *35*, 325–336.

Weibull, W. (1951). A statistical distribution function of wide applicability. *Journal of Applied Mechanics*, *18*, 293–297.

Wichmann, F. A., & Hill, N. J. (2011). The psychometric function: I. Fitting, sampling, and goodness of fit. *Attention, Perception, & Psychophysics*, *63*, 1293–1313.

Xu, X., Anderson, T. J., & Casagrande, V. A. (2007). How do functional maps in primary visual cortex vary with eccentricity? *Journal of Comparative Neurology*, *501*, 741–755.

Yu, H. H., Verma, R., & Yang, Y., Tibballs, H. A., Lui, L. L., Reser, D. H., & Rosa, M. G. (2010). Spatial and temporal frequency tuning in striate cortex: Functional uniformity and specializations related to receptive field eccentricity. *European Journal of Neuroscience*, *31*, 1043–1062.